Large Eddy Simulation of the Gas–Liquid Flow in a Stirred Tank

Yanhong Zhang
Key Laboratory of Green Process and Engineering, Institute of Process Engineering, Chinese Academy of Sciences, Beijing 100190, China, and
Key Lab of Safety Science of Pressurized System, Ministry of Education School of Mechanical Engineering, East China University of Science and Technology, Shanghai 200237, China

Chao Yang
Key Laboratory of Green Process and Engineering, Institute of Process Engineering, Chinese Academy of Sciences, Beijing 100190, China, and
Jiangsu Institute of Marine Resource Exploitation, Lianyungang 222005, China

Zai-Sha Mao
Key Laboratory of Green Process and Engineering, Institute of Process Engineering, Chinese Academy of Sciences, Beijing 100190, China

DOI 10.1002/aic.11516
Published online May 22, 2008 in Wiley InterScience (www.interscience.wiley.com).

Both the large eddy simulation (LES) technique and the k-ε turbulent model were used to simulate the gas-liquid turbulent flow in a stirred tank driven by a Rushton impeller. A Eulerian-Eulerian two-fluid model for gas–liquid two-phase flow was developed using the large eddy simulation for both gas and liquid phases. The relative movement of the rotating impeller to the static baffles was accounted for through the improved inner-outer iterative algorithm. The spatial discretization of the governing equations was performed on a cylindrical staggered grid. For the LES, a conventional Smagorinsky sub-grid model was adapted to modeling the turbulence of the liquid phase. The momentum and continuity equations were discretized using the finite difference method, with a third order QUICK (Quadratic Upwind Interpolation for Convective Kinematics) scheme used for convective terms. The phase-resolved predictions of the LES were compared with the experimental data and the simulation results by the standard k-ε model, suggesting that the LES has much better accuracy than the *k-ε* model. © 2008 American Institute of Chemical Engineers *AIChE J,* 54: 1963–1974, 2008
Keywords: large eddy simulation, gas–liquid flow, stirred tank, computational fluid dynamics, turbulence

Introduction

Gas–liquid stirred reactors are widely used in chemical and biochemical industry. Many efforts have been made in simulation of the gas–liquid flows in stirred tanks. Gosman et al.[1] firstly extended the simulation of two-phase flow from two-dimensional to three-dimensional cases with a simplified equation of the gas momentum and the impeller zone was dealt as a black box. Bakker and van den Akker[2] assumed that there was little effect of the gas on the liquid phase and simulated the gas–liquid flow in a stirred tank with different impellers including Rushton impeller, pitched-blade impeller, and A315 impeller. In comparison with the experimental data measured by themselves, the prediction was rather poor and the authors attributed it to the treatment of the impeller zone as a black box. Ranade and van den Akker[3] used the two-fluid model to describe the gas–liquid flow and the movement of the impeller relative to the baffles was modeled by the snapshot method.

Correspondence concerning this article should be addressed to C. Yang at chaoyang@home.ipe.ac.cn, or Z.-S. Mao at zsmao@home.ipe.ac.cn.

Morud and Hjertager[4] simulated the two-dimensional gas–liquid flow in a stirred tank employing the black box approach, too. Ranade and Deshpande[5] studied the trailing vortex behind an impeller by the snapshot method. Mao and coworkers[6,7] employed the improved inner-outer iterative algorithm and the two-fluid model to simulate the gas–liquid flow in a three-dimensional stirred tank. Lane et al.[8,9] predicted the gas–liquid flow in a stirred tank using a multiple frames of reference method to account for the relative movement of the impeller with the consideration of coalescence and break-up of the bubbles. Khopkar et al.[10,11] applied the two-fluid model and snapshot method to simulate the gas–liquid flow in stirred tanks. Deen et al.[12] employed a sliding mesh method to simulate the interaction between the impeller and the baffles using a CFD package. Sun et al.[13] extended the two-fluid model and the improved inner-outer iterative algorithm to the gas–liquid flow in surface aerated stirred tanks.

Although the large eddy simulation was successfully applied in the single phase simulation in stirred tanks,[14–20] to date there is no work published on studying the gas–liquid flow in stirred tanks using the large eddy simulation (LES). Several groups[21–24] have attempted to apply the large eddy simulation to the two-phase flow, but in all of these papers the Lagrangian frame of reference were employed to model the disperse phase. The only study on the flow in a stirred tank using LES is by Derksen,[25] who simulated the liquid–solid flow describing the solid phase also by the Lagrangian frame. As to the engineering application, the Eulerian formulation is preferred. Up to now, only Smith and Milelli[26] and Deen et al.[27] applied a combination of the large eddy simulation and the Eulerian-Eulerian two phase flow approach to simulate the gas–liquid phase flow.

In this work, we used two different models for turbulent viscosity, i.e., LES model and standard k-ε model. The Eulerian-Eulerian approach is used to describe the gas–liquid two-phase flow. The relative movement between the rotating impeller and the static wall baffles was accounted for through the improved inner–outer iterative algorithm.[6] This article is the first attempt to apply the large eddy simulation to a gas-sparged stirred tank.

Mathematical Model

Governing equations

The instantaneous equations for phase m (gas or liquid phase) in an Eulerian-Eulerian formulation are generally given as follows:

Continuous equation

$$\frac{\partial(\rho_m\alpha_m)}{\partial t}+\frac{\partial}{\partial x_j}\left(\rho_m\alpha_m u_{m,i}\right)=0 \tag{1}$$

Momentum equation

$$\frac{\partial}{\partial t}\left(\rho_m\alpha_m u_{mi}\right)+\left(\frac{\partial}{\partial x_j}\left(\rho_m\alpha_m u_{mi}u_{mj}\right)\right)=-\alpha_m\frac{\partial(p)}{\partial x_i}+\rho_m x_m g_i + F_{mi}+\frac{\partial}{\partial x_j}\left(\mu_m\left(\frac{\partial\left(\alpha_m u_{mj}\right)}{\partial x_i}+\frac{\partial(\alpha_m u_{mi})}{\partial x_j}\right)\right) \tag{2}$$

where u_{mi}, α_m are the instantaneous velocity components and phase volume fraction for phase m, respectively, and F_{mi} is the inter-phase momentum exchange terms.

The transport equations of k and ε for the standard k-ε model can be written as

$$\frac{\partial}{\partial t}\left(\rho_m\alpha_m k\right)+\frac{\partial}{\partial x_j}\left(\rho_m\alpha_m u_{mi}k\right)=\frac{\partial}{\partial x_j}\left(\alpha_m\frac{\mu_t}{\sigma_k}\frac{\partial k}{\partial x_j}\right)+\alpha_m(G-\rho_m\varepsilon) \tag{3}$$

$$\frac{\partial}{\partial t}\left(\rho_m\alpha_m\varepsilon\right)+\frac{\partial}{\partial x_j}\left(\rho_m\alpha_m u_{mi}\varepsilon\right)=\frac{\partial}{\partial x_j}\left(\alpha_m\frac{\mu_t}{\sigma_\varepsilon}\frac{\partial\varepsilon}{\partial x_j}\right)+\alpha_m\frac{\varepsilon}{k}\left(C_1(G+G_{\mathrm{e}})-C_2\rho_{\mathrm{m}}\varepsilon\right) \tag{4}$$

$$G_{\mathrm{e}}=C_{\mathrm{b}}|F_{mi}|\left(\sum\left(u_{\mathrm{li}}-u_{gi}\right)^2\right)^{\frac{1}{2}} \tag{5}$$

$$\mu_t=C_\mu\frac{k^2}{\varepsilon} \tag{6}$$

where G_{e} represents the effect of bubbles on energy dissipation. C_{b} is an experiential parameter, which is taken as 0.02.[28] C_μ, σ_k, and σ_ε are empirical constants recommended by Launder and Spalding[29]:

$$C_\mu=0.09,\quad C_1=1.43,\quad C_2=1.92,\quad \sigma_k=1.0,\quad \sigma_\varepsilon=1.3$$

G is the turbulence generation rate:

$$G=2\mu_{\mathrm{lt}}\left[\left(\frac{\partial u_{lr}}{\partial_r}\right)^2+\left(\frac{1}{r}\frac{\partial u_{l\theta}}{\partial\theta}+\frac{\mu_{lr}}{r}\right)^2+\left(\frac{\partial u_{lz}}{\partial z}\right)^2\right]+\mu_{\mathrm{lt}}\left[r\frac{\partial}{\partial r}\left(\frac{u_{l\theta}}{r}\right)+\frac{1}{r}\frac{\partial u_{lr}}{\partial\theta}\right]^2+\mu_{\mathrm{t}}\left(\frac{\partial u_{l\theta}}{\partial z}+\frac{1}{r}\frac{\partial u_{lz}}{\partial\theta}\right)^2+\mu_{\mathrm{t}}\left(\frac{\partial u_{lz}}{\partial r}+\frac{\partial u_{lr}}{\partial z}\right)^2 \tag{7}$$

For the LES, the space-filtered equations for the conservation of mass and momentum of an incompressible Newtonian fluid can be written as

$$\rho_m\frac{\partial(\bar{\alpha}_m)}{\partial t}+\rho_m\frac{\partial}{\partial x_j}\left(\overline{\alpha_m u_{mi}}\right)=0 \tag{8}$$

$$\frac{\partial}{\partial t}\left(\rho_m\overline{\alpha_m u_{mi}}\right)+\left(\frac{\partial}{\partial x_j}\left(\rho_m\overline{\alpha_m u_{mi}u_{mj}}\right)\right)=-\frac{\partial(\bar{p})}{\partial x_i}+\rho_m\overline{\alpha}_m g_i+\bar{F}_{mi}+\frac{\partial}{\partial x_j}\left(\mu_m\left(\frac{\partial\left(\overline{\alpha_m u_{mj}}\right)}{\partial x_i}+\frac{\partial\left(\overline{\alpha_m u_{mi}}\right)}{\partial x_j}\right)\right). \tag{9}$$

The relationships between the variables in Eqs. 2 and 9 are

$$u_{mj}=\bar{u}_{\bar{m}j}+u'_{mj} \tag{10}$$

$$\alpha_m=\bar{\alpha}_m+\alpha'_m \tag{11}$$

$$p=\bar{p}+p \tag{12}$$

where $\bar{\varphi}(\varphi=u_{mj},\alpha_m,p)$ represents the part that will be resolved in the simulation and φ' the unresolved part on a

scale smaller than the mesh. So, Eqs. 8 and 9 can be rewritten as

$$\frac{\partial(\rho_m\bar{\alpha}_m)}{\partial t}+\frac{\partial}{\partial x_j}\left(\rho_m\bar{\alpha}_m\bar{u}_{mj}\right)+\frac{\partial}{\partial x_j}\left(\rho_m\overline{\alpha'_m u'_{mj}}\right)+\frac{\partial}{\partial x_j}\left(\rho_m\overline{\alpha'}_m\bar{u}_{mj}\right)+\frac{\partial}{\partial x_j}\left(\rho_m\bar{\alpha}_m\overline{u'_{mj}}\right)=0 \quad (13)$$

$$\frac{\partial}{\partial t}\left(\rho_m\bar{\alpha}_m\bar{u}_{mi}\right)+\frac{\partial}{\partial t}\left(\rho_m\overline{\alpha'_m u'_{mi}}\right)+\frac{\partial}{\partial t}\left(\rho_m\overline{\alpha'_m}\bar{u}_{mi}\right)+\frac{\partial}{\partial t}\left(\rho_m\bar{\alpha}_m\overline{u'_{mi}}\right)+\frac{\partial}{\partial x_j}\left(\rho_m\bar{\alpha}_m\overline{u_{mi}u_{mj}}+\rho_m\overline{\alpha'_m u_{mi}u_{mj}}\right)=-\frac{\partial(\bar{p})}{\partial x_i}+\rho_m\bar{\alpha}_m g_i+\bar{F}_{mi}+\mu_m\frac{\partial}{\partial x_j}\left(\frac{\partial(\bar{\alpha}_m\bar{u}_{mj})}{\partial x_i}+\frac{\partial(\bar{\alpha}_m\bar{u}_{mi})}{\partial x_j}\right)+\mu_m\frac{\partial}{\partial x_j}\left(\frac{\partial(\overline{\alpha'}_m\bar{u}_{mj}+\bar{\alpha}_m\overline{u'_{mj}})}{\partial x_i}+\frac{\partial(\overline{\alpha'}_m\bar{u}_{mi}+\bar{\alpha}_m\overline{u'_{mi}})}{\partial x_j}\right). \quad (14)$$

The unresolved parts of the numerical simulations are the fluctuating velocity and holdup, which have to be omitted because there are no proper closing methods yet. The mean and the fluctuating velocities are the grid scale and the subgrid scale terms through a filtering operation. The terms with $\overline{u_{mi}u_{mj}}$ are formulated by a LES subgrid model. Omitting the terms with the α'_m and u'_{mi}, the above equations become

$$\frac{\partial(\rho_m\bar{\alpha}_m)}{\partial t}+\frac{\partial}{\partial x_j}\left(\rho_m\bar{\alpha}_m\bar{u}_{mj}\right)=0 \quad (15)$$

$$\frac{\partial}{\partial t}\left(\rho_m\bar{\alpha}_m\bar{u}_{mi}\right)+\frac{\partial}{\partial x_j}\left(\rho_m\bar{\alpha}_m\bar{u}_{mi}\bar{u}_{mj}\right)=-\frac{\partial(\bar{p})}{\partial x_i}+\rho_m\bar{\alpha}_m g_i+\bar{F}_{mi}+\mu_m\frac{\partial}{\partial x_j}\left(\frac{\partial\left(\bar{\alpha}_m\bar{u}_{mj}\right)}{\partial x_i}+\frac{\partial(\bar{\alpha}_m\bar{u}_{mi})}{\partial x_j}\right)-\frac{\partial\left(\rho_m\bar{\alpha}_m\tau_{mij}\right)}{\partial x_j} \quad (16)$$

$$\tau_{mij}=\overline{u_{mi}u_{mj}}-\bar{u}_{mi}\bar{u}_{mj} \quad (17)$$

where τ_{mij} is the subgrid scale stress tensor, which reflects the effect of the unresolved scales on the resolved scales. In this work, the effect of the sub-grid scales on the large scales of the liquid phase is accounted for based on the standard Smagorinsky model[30]:

$$\tau_{lij}-\frac{1}{3}\tau_{lkk}\delta_{ij}=-(c_s\Delta)^2\left|\overline{S_l}\right|\bar{S}_{lij} \quad (18)$$

with the eddy viscosity defined as

$$\nu_{lt}=(c_s\Delta)^2\left|\overline{S_l}\right| \quad (19)$$

$$\left|\overline{S_l}\right|=\left(2\bar{S}_{lij}\bar{S}_{lij}\right)^{\frac{1}{2}} \quad (20)$$

$$\bar{S}_{lij}=\frac{1}{2}\left(\frac{\partial\bar{u}_{li}}{\partial x_j}+\frac{\partial\bar{u}_{lj}}{\partial x_i}\right). \quad (21)$$

Here, a value of 0.1 was adapted for c_s.

The effective gas viscosity is calculated based on the following formula:

$$\mu_{\mathrm{eff},g}=\frac{\rho_g}{\rho_l}\mu_{\mathrm{eff},l}. \quad (22)$$

The inter-phase coupling terms make the two-phase flow fundamentally different from the single-phase flow. F_{mi} satisfies the following relation:

$$F_{l,i}=-F_{g,i} \quad (23)$$

where subscripts l and g denote liquid and gas phase, respectively. For the dispersed two-phase flow, $F_{m,i}$ mainly consists of four terms: the inter-phase drag force, the virtual mass force, the Basset force, and the lift force. In most cases, the magnitude of the Basset force and lift force are much smaller than that of the inter-phase drag force. The virtual mass force will be significant in the gas-liquid flows with large accelerations such as the flow in bubble columns; however, the gas hold-up values for the stirred vessels are usually rather low. Compared to the drag force, the lift force and the virtual mass force have little influence.[3] Gosman et al.[1] examined the effects of the inter-phase forces by an order of magnitude analysis, the conclusion was that the lift force and the virtual mass force were much less significance compared to the drag force in the stirred vessels. Recent report by Khopkar et al.[11] also indicated that the effect of the virtual mass force is not significant in the bulk region of the stirred tank. So only the inter-phase drag force was included in the momentum

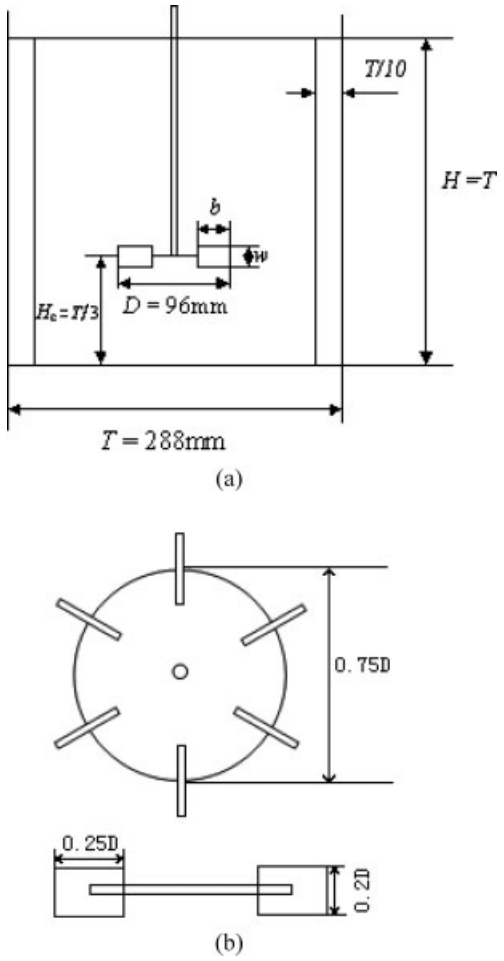

Figure 1. (a) The geometry of the tank; (b) Rushton impeller.

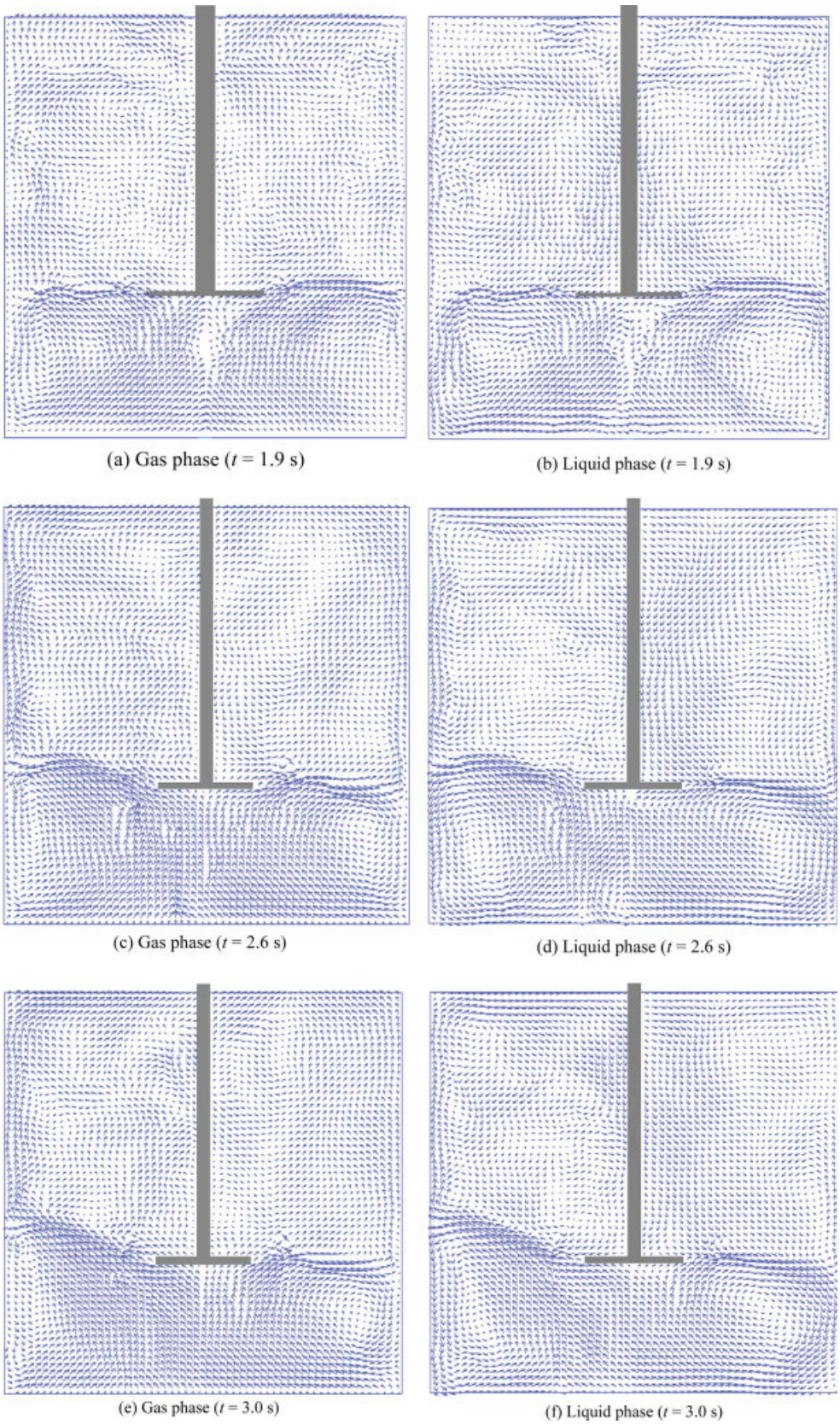

Figure 2. Instantaneous velocity fields in *r-z* plane at three different instants by the LES (ω = 41.9 rad/s).

(a) Gas phase (t = 1.9 s); (b) Liquid phase (t = 1.9 s); (c) Gas phase (t = 2.6 s); (d) Liquid phase (t = 2.6 s); (e) Gas phase (t = 3.0 s); (f) Liquid phase (t = 3.0 s). [Color figure can be viewed in the online issue, which is available at www.interscience.wiley.com.]

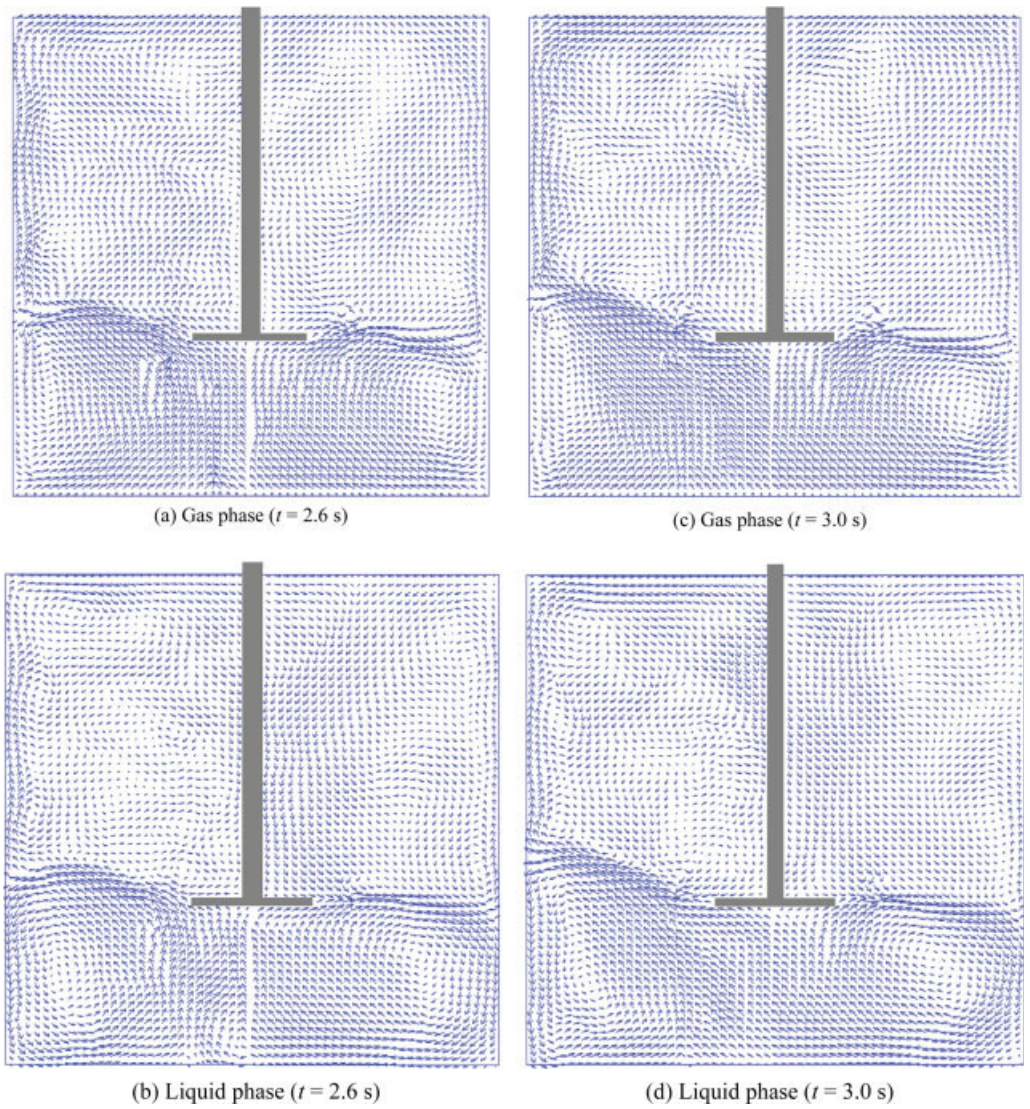

Figure 3. Instantaneous velocity field in *r–z* plane at two different instants by the LES (ω = 62.8 rad/s).

(a) Gas phase (t = 2.6 s); (b) Liquid phase (t = 2.6 s); (c) Gas phase (t = 3.0 s); (d) Liquid phase (t = 3.0 s). [Color figure can be viewed in the online issue, which is available at www.interscience.wiley.com.]

equations. In a non-inertial reference frame, there are also the centrifugal force $\mathbf{F}_{r,m}$ and the Coriolis force $\mathbf{F}_{c,m}$, which could be written as

$$\text{centrifugal force}: \quad \mathbf{F}_{r,m} = \alpha_m \rho_m (\boldsymbol{\omega} \times \mathbf{r}) \times \omega \tag{24}$$

$$\text{Coriolis force}: \quad \mathbf{F}_{c,m} = 2\alpha_m \rho_m \boldsymbol{\omega} \times \mathbf{u}_m \tag{25}$$

Drag coefficient

The inter-phase drag force exerted on the gas phase is given by

$$\overline{F}_{\mathrm{g},l} = -\frac{3\alpha_\mathrm{g}\alpha_l\rho_l C_\mathrm{D}}{4d_b}\left(\sum_{i=1}^{3}(\bar{u}_{g,i}-\bar{u}_{li})^2\right)^{0.5}(\bar{u}_{\mathrm{g},i}-\bar{u}_{l,i}) \tag{26}$$

where C_D, the inter-phase drag coefficient, is a complex function on gas hold-up and turbulence intensity. We use the correlation recommended by Brucato et al.[31] with the empirical constant of 6.5×10^{-6} recommended by Lane et al.[32]:

$$\frac{C_\mathrm{D} - C_{\mathrm{D0}}}{C_{\mathrm{D0}}} = 6.5 \times 10^{-6}\left(\frac{d_\mathrm{b}}{\lambda}\right)^3 \tag{27}$$

$$C_{\mathrm{D0}} = \max\left\{\left(\frac{2.667Eo}{Eo+4.0}\right), \quad \left(\frac{24}{Re_\mathrm{b}}\right)\left(1+0.15Re_\mathrm{b}^{0.687}\right)\right\} \tag{28}$$

$$Re_\mathrm{b} = \frac{d_\mathrm{b}\rho_l}{\mu_{l,\mathrm{lam}}}\left(\sum\left(\bar{u}_{g,i}-\bar{u}_{l,i}\right)^2\right)^{0.5} \tag{29}$$

$$\lambda = \left(\frac{\nu_l^3}{\varepsilon_l}\right)^{0.25} \tag{30}$$

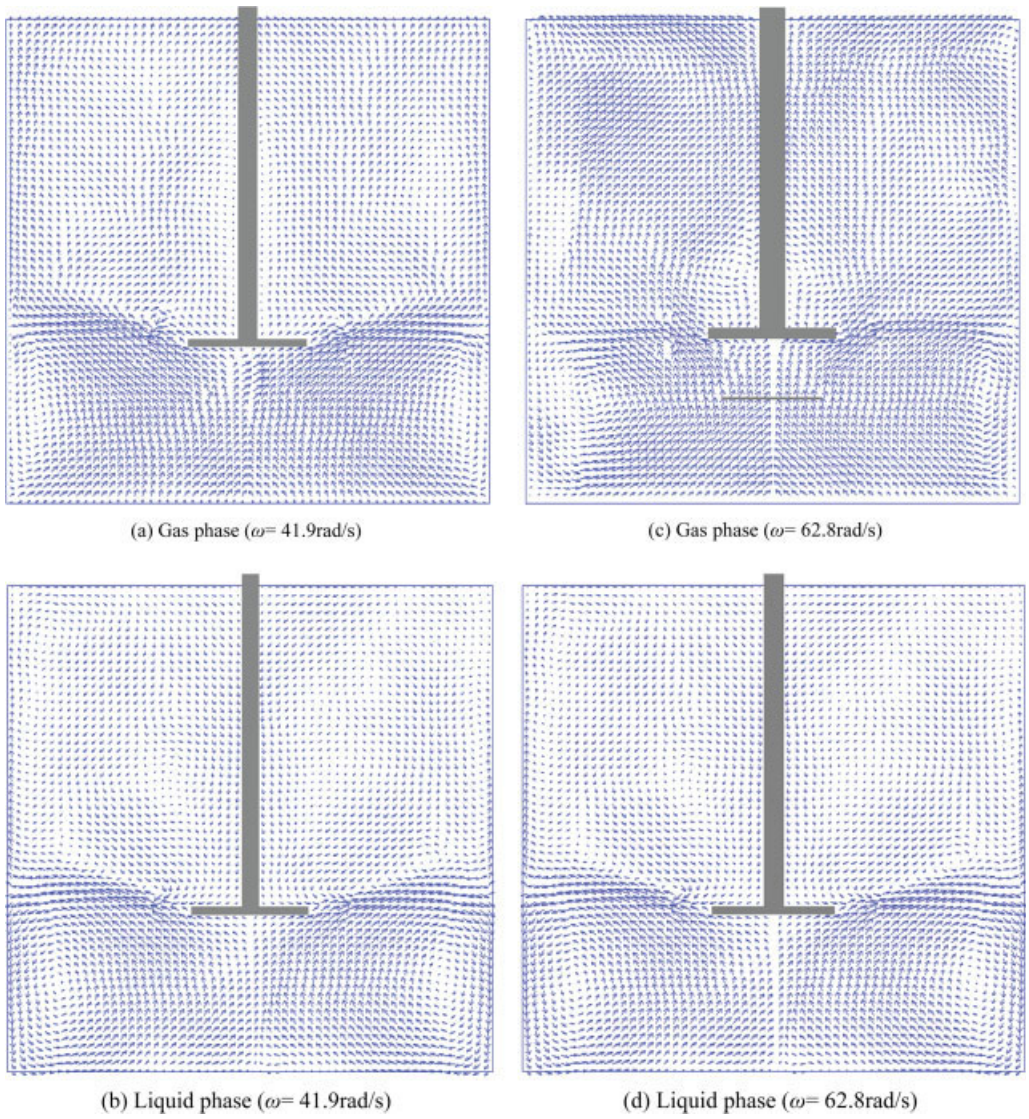

Figure 4. Phase-resolved velocity fields in *r–z* plane by the LES.

(a) Gas phase (ω = 41.9 rad/s); (b) Liquid phase (ω = 41.9 rad/s); (c) Gas phase (ω = 62.8 rad/s); (d) Liquid phase (ω = 62.8rad/s). [Color figure can be viewed in the online issue, which is available at www.interscience.wiley.com.]

$$d_{\mathrm{b}} = 0.68 \times 0.725\left(\frac{\sigma}{\rho_l}\right)^{0.6} \times \varepsilon_l^{-0.4} \quad [11] \tag{31}$$

where d_{b} is the bubble diameter, λ the Kolmogoroff microscale of dissipative eddies, and $\mu_{\mathrm{l,lam}}$ the laminar viscosity of the liquid. The above correlation takes account of the effect of turbulence on the drag force of gas bubbles. Equation 31 introduces the effect of the turbulence on the bubble size distribution, but in the predicted results the bubble size is actually in a narrow range about 5 mm.

Numerical Method

The geometry of the stirred tank simulated in this work is depicted in Figure 1, consisting of a cylindrical tank with a standard six-blade Rushton turbine and four baffles on the tank wall, as the same as that tested by Lu and Ju.[33] The tank was filled with water at room temperature. A perforated ring of 8 cm diameter steel tube was placed 3.5 cm below the impeller as the sparger, on which the holes of 2 mm diameter were drilled every 2 cm. The gas flow rate was 3.43×10^{-4} m^3 s^{-1}. Simulations were made for two impeller rotating speeds (41.9 and 62.8 rad/s corresponding to the Reynolds numbers of 9.2×10^4 and 6.9×10^4, and the tip velocities u_{tip} of 3.0 m s^{-1} and 2.3 m s^{-1}, respectively).

Except the axial component of the liquid velocity, the free surface boundary condition was applied to all the variables including k and ε. The normal liquid velocity fell to zero at the top free surface. The gas bubbles were free to escape from the top surface. At all solid surfaces, no-slip boundary conditions were enforced. An asymmetric boundary condition[20]

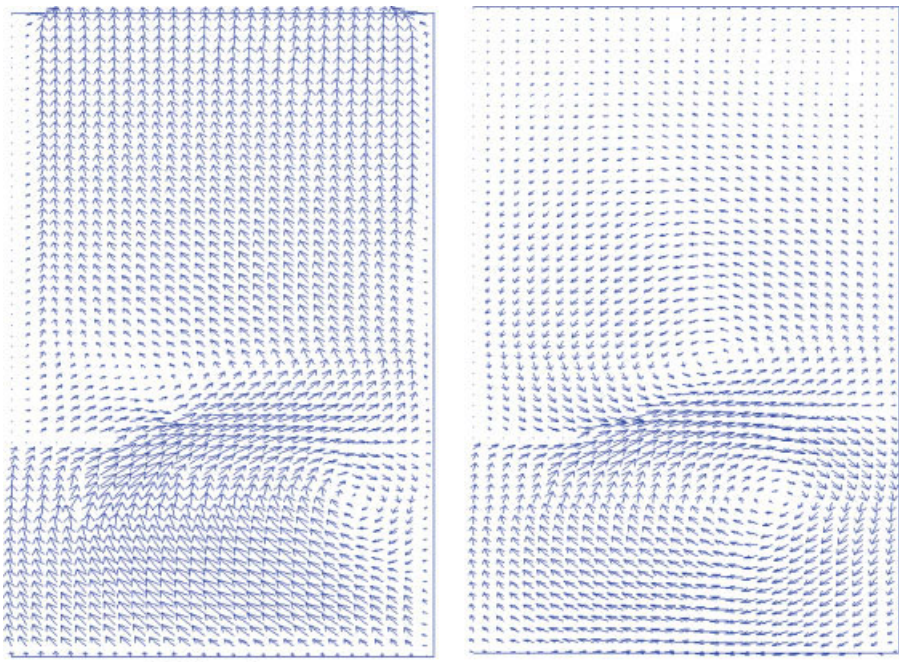

Figure 5. Velocity vector plots predicted by the standard *k*–ε model (ω = 41.9 rad/s).

(a) Gas phase; (b) Liquid phase. [Color figure can be viewed in the online issue, which is available at www.interscience.wiley.com.]

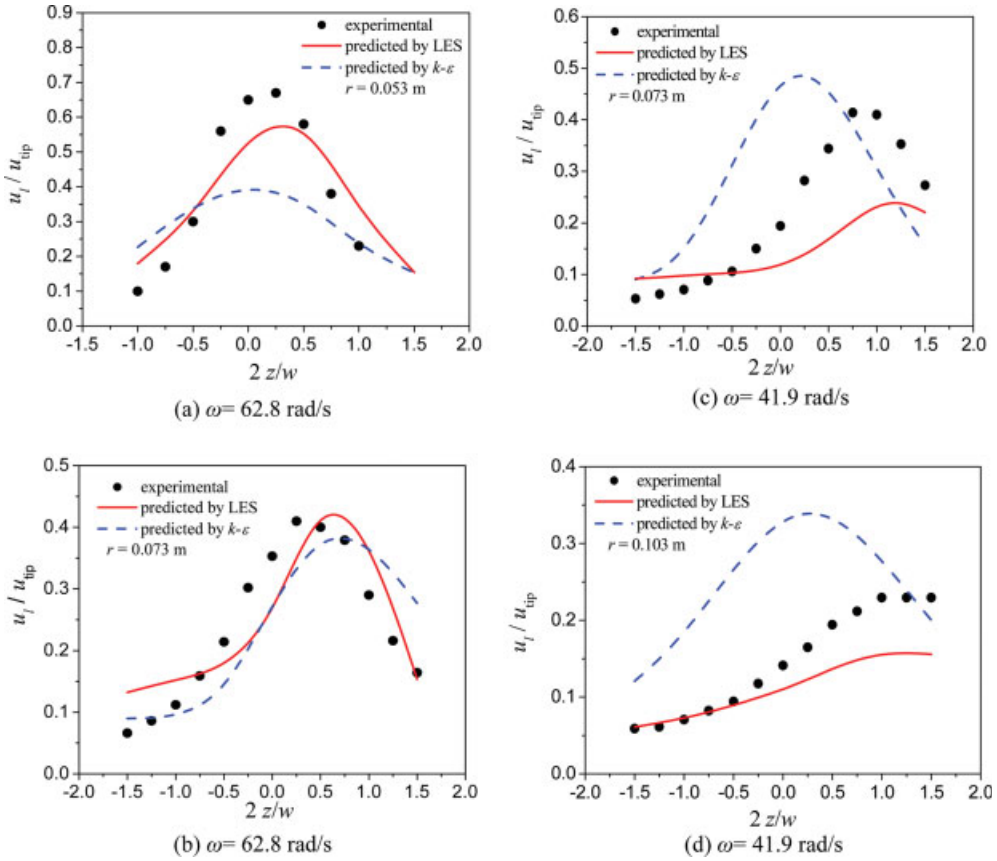

Figure 6. Predicted liquid velocity profiles by the LES compared with the experimental data by Lu and Ju[33] and the standard *k*–ε model prediction at different radial positions.

(a) ω = 62.8 rad/s; (b) ω = 62.8 rad/s; (c) ω = 41.9 rad/s; (d) ω = 41.9 rad/s. [Color figure can be viewed in the online issue, which is available at www.interscience.wiley.com.]

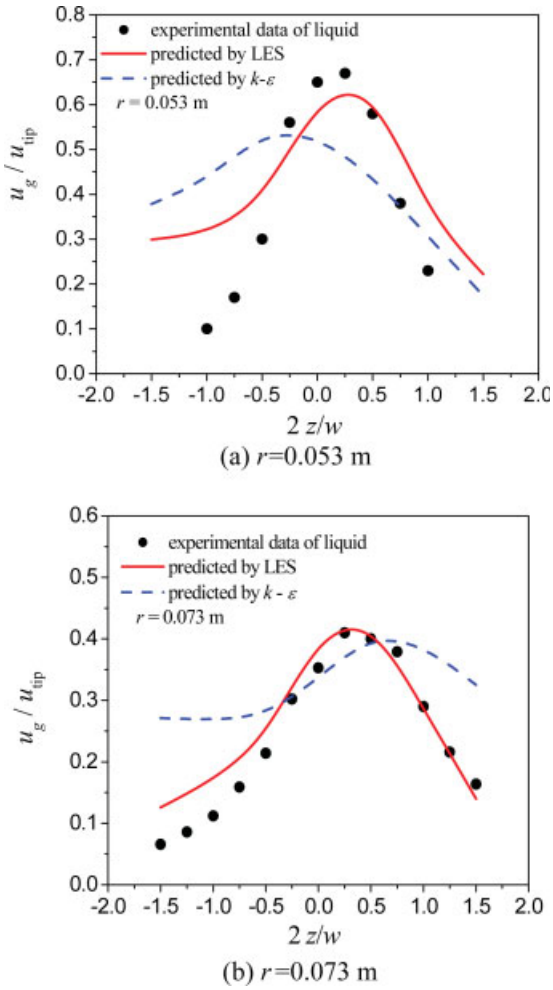

Figure 7. Predicted Gas velocity profiles by the LES compared with the experimental data of liquid phase by Lu and Ju[33] and the standard *k*-ε model prediction at different radial positions (ω = 62.8 rad/s).

(a) r = 0.053 m; (b) r = 0.073 m. [Color figure can be viewed in the online issue, which is available at www.interscience.wiley.com.]

was enforced at the axis below the impeller to allow the possible flow across the axis.

The tank was modeled with a uniform grid in cylindrical coordinates. The discretization of the partial differential equations was achieved by control volume formulation with a staggered arrangement of primary variables, and then the pressure-velocity coupling was dealt with the SIMPLE algorithm.[34] In the LES, high-order accuracy was needed to decrease the numerical dissipation. To avoid the physical phenomena being masked, a third-order QUICK scheme was used for convective terms and a second-order central scheme for diffusive terms. The time integration was discretized by a Crank-Nicolson implicit scheme.

The implementation of the modified inner-outer iterative procedures was involved with the numerical solution of the governing equations in the inner zone including the impeller swept region in the rotating non-inertial reference frame and that in the outer zone excluding the impeller region in a fixed inertial reference frame.[6] The matching of the flow parameters at the overlapping parts of the inner and outer zones was necessary for each iteration to advance a time step.

The large eddy simulation was started from the velocity field from the *k*-ε model simulation with the time step of 1.0×10^{-4} s. A computational domain consisting of $60 \times 48 \times 60$ control volumes was defined for the case of ω = 62.8 rad/s and $60 \times 72 \times 120$ for ω = 41.9 rad/s. The blade thickness was chosen to be the size of a mesh. Normally after 1 s, a stabilized flow field was achieved. In the following 2.5 s, the flow field data were collected and processed. The instantaneous values were averaged to obtain the phase-resolved vector fields.

The in-house computer code was compiled in FORTRAN and was run on a PC computer with P4 CPU 2.80 GHz. A typical job using the $60 \times 48 \times 60$ grid took about 30 days of CPU time, which is longer than that in the large eddy simulation of single phase flow with a $120 \times 120 \times 120$ grid.[20]

Results and Discussion

In this work, the simulations of a gas-liquid tank stirred by a Rushton impeller have been carried out for two turbulent models. For the *k*-ε model simulation, only half of the tank was simulated, because the time-independent two-phase flow was sought.

Flow map

Figures 2 and 3 show the instantaneous velocity vector maps of the gas and liquid phases in the *r*-*z* plane located midway between two blades at three different time instants, 1.9, 2.6 and 3.0 s, respectively. We can see clearly that the flow pattern in a gas spargered tank is very complex, which could not be well predicted by the *k*-ε model. There are many small vortexes in both the gas and the liquid flow fields and the flow patterns change with the time. The flow in the tank is not symmetrical as most work presumed to be.

Figure 4 shows the phase-resolved vector fields of the gas and liquid phases in the *r*-*z* plane located midway between two blades. From the liquid vector map we can find that the jets by the impeller are slightly upward inclined due to the movement of the gas phase. Because part of the gas is sucked back to the tank at the free surface, two small liquid circulation rings appear just below the liquid surface and near the wall. Compared with the flow maps of the liquid phase, the large vortex in the under recirculation zones are much closer to the wall. Different from the instantaneous velocity fields, the phase-resolved velocity fields are basically symmetrical except the place under the impeller disc, where there are fluid flows across the axis.

Figure 5 shows the velocity vector plots simulated by the *k*-ε model in the same plane as in the Figure 4. Both the two models give the similar time-averaged velocity vector fields.

Phase-resolved velocity

Figures 6 and 7 shows the profiles of the phase-resolved resultant velocities at different radial positions in contrast to the experimental data of liquid resultant velocity. It can be

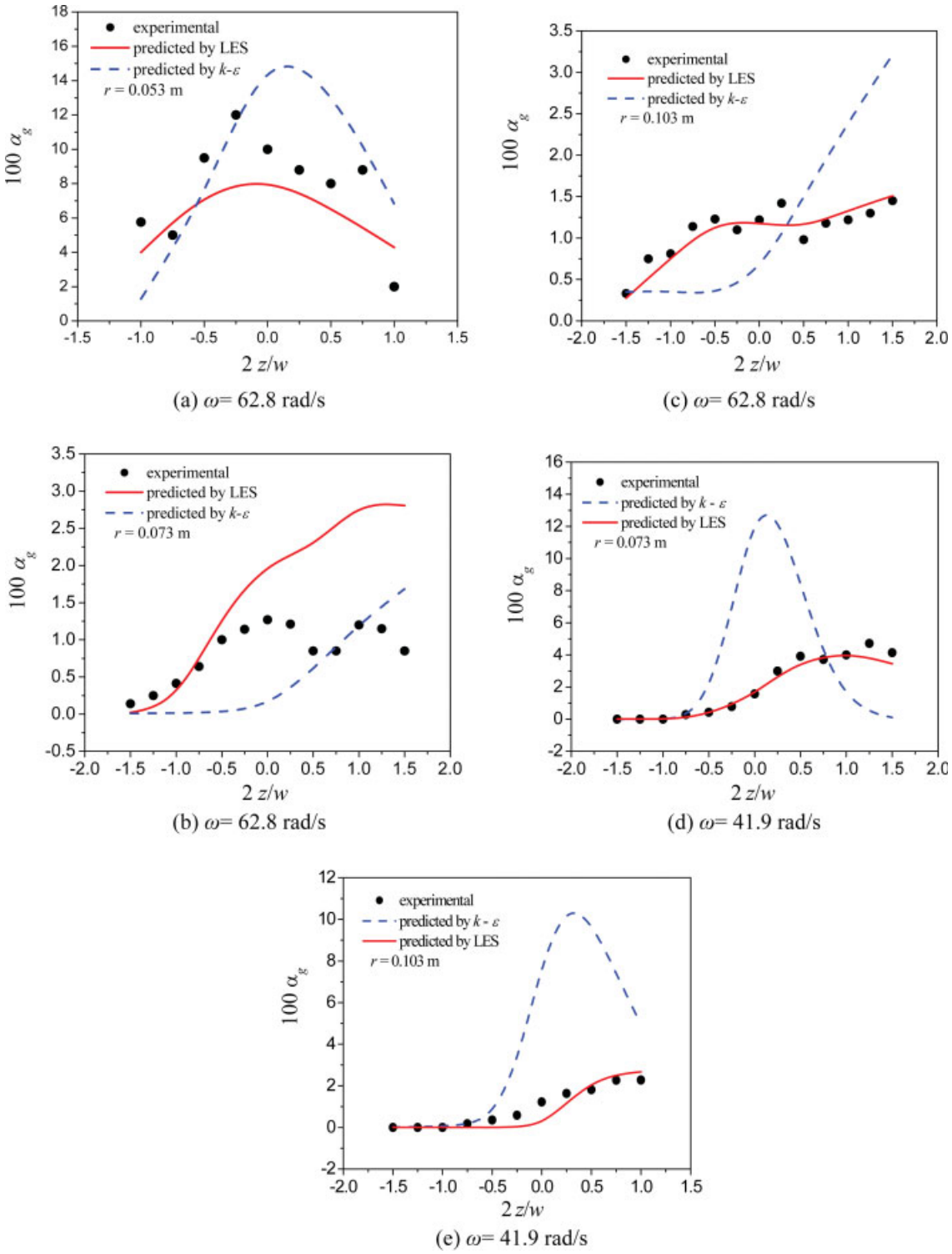

Figure 8. Predicted Gas holdup profiles by the LES compared with the experimental data by Lu and Ju[33] and the standard *k–ε* model prediction at different radial positions.

(a) ω = 62.8 rad/s; (b) ω = 62.8 rad/s; (c) ω = 62.8 rad/s; (d) ω = 41.9 rad/s; (e) ω = 41.9 rad/s. [Color figure can be viewed in the online issue, which is available at www.interscience.wiley.com.]

seen clearly that the predicted maximum velocity values deviate from the experimental nearby the impeller disc. Because of the movements of the gas bubbles and the up decline of the liquid jets, the further the position is from the impeller, the more the deviation of the predicted velocity is. As the gas–liquid turbulent flow in a stirred tank is very complex and difficult to be measured especially at high gas holdup, few experiments are reported on gas or liquid velocity

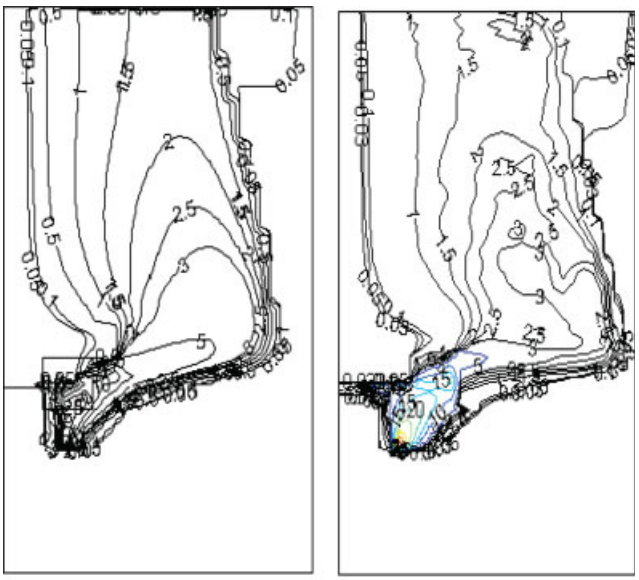

(a) standard k-ε model (b) LES

Figure 9. Averaged volume fraction of gas in the *r–z* plane between blades (ω = 41.9 rad/s).

(a) standard k-ε model; (b) LES. [Color figure can be viewed in the online issue, which is available at www.interscience.wiley.com.]

field and phase holdup. In comparison to the predictions by the k-ε model, these from the LES are more fitted to the experimental data of Lu and Ju,[31] especially in the position near the impeller tips. This is because that the flow in the impeller zone is the most complex in the tank, which is three-dimensional and anisotropic. The k-ε model is unable to simulate the strongly anisotropic flow well because it is established on the basis of the assumption of isotropic turbulent flow.

Up to now, there are seldom experimental velocity data of the gas phase in multiphase flow in a stirred tank. It is expected that the trends of variation of the velocities of two phases are consistent considering the intensive interaction between the gas and the liquid phase. Near the impeller, the gas velocity shall be greater than that of the liquid phase because of the effect of buoyancy of bubbles. The farther is the location from the impeller, the closer are the velocities of the two phases.

Gas holdup

Figure 8 shows the profiles of the phase-resolved velocities at positions r = 0.053 m, r = 0.073 m, and r = 0.103 m. The predicted holdups by the LES agree better with the experimental values than those by the k-ε model. However, there are still great deviations between the predictions and the measurements, because that there is no any proper model to describe accurately the very complex two-phase flow in the impeller zone.

Figure 9 shows the contours of the gas holdup in the r-z plane located midway between two blades predicted by the LES and the k-ε model, respectively. Because some gas bubbles are inhaled by the impeller, the isolines of the gas holdup around the blades are very close. In the bulk flow, the results of the two turbulent models give very similar patterns of gas holdup distribution. In the swept region, however, the k-ε model gives bigger values than the LES does as showed in Figure 8.

Energy dissipation is an important quantity in a stirred tank since it provides a direct measure of energy input into

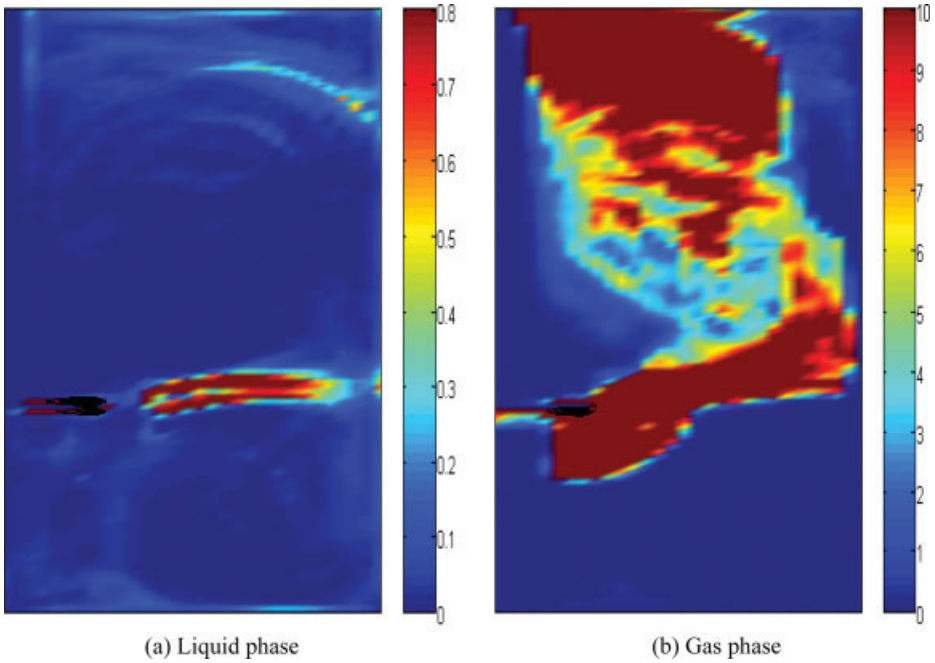

(a) Liquid phase (b) Gas phase

Figure 10. Phase-resolved energy dissipation ε(m^2/s^3) in the plane between two impeller blades by the LES (ω = 41.9 rad/s).

(a) Liquid phase; (b) Gas phase. [Color figure can be viewed in the online issue, which is available at www.interscience.wiley.com.]

the system at the impeller. In the context of LES, the total dissipation is given by[35]

$$\langle \varepsilon \rangle = \left\langle 2(\nu_t + \nu)|\overline{S}|^2 \right\rangle \tag{32}$$

where $\langle\ \rangle$ designates a statistical average over the whole tank.

Figure 10 presents the distribution of the energy dissipation per mass of fluid in the plane midway between two successive blades throughout the tank. The energy dissipation of liquid phase is mainly concentrated in the impeller swept region and in the impeller outflow. Very high dissipation rates are located at the blade edges and near the wake of the blades. The zone of high dissipation rate is smaller than that in the single phase,[20] which shows that the existence of the bubbles suppresses the production of turbulence. It is interesting to notice that the zone of high energy dissipation of gas is rather large, both in the impeller outflow and in the upper part of the upper bulk circulation zone. It seems that the behavior is closely related with the large velocity of interphase slip.

Conclusions

The LES turbulent model has great potential in understanding the fluid flow behaviors. In this article, a Eulerian-Eulerian two-fluid model for gas-liquid two-phase flow was first developed using the large eddy simulation for both gas and liquid phases in a three-dimensional frame.

A conventional Smagorinsky sub-grid model was adapted to modeling the turbulence of the liquid phase, with a third order QUICK scheme used for convective terms. The relative movement between the rotating impeller and the static baffles was accounted for through the improved inner-outer iterative algorithm. The spatial discretization of the governing equations was performed on a cylindrical staggered grid. A k-ε model was also carried out for the purpose of the comparison to the LES.

The complex flow pattern of gas-liquid flow in a gas sparged tank was well predicted. There are many small vortexes in both the gas and the liquid flow fields and the flow patterns change with the time. The flow in the tank is not symmetrical as most work presumed to be. The phase-resolved predictions of the LES were compared with the experimental data and the results by k-ε model suggesting that LES is much better than the k-ε model. The present study has shown the suitability of the LES coupled with a two-fluid model for simulating the gas–liquid flow in a stirred tank.

Because much computer time is needed in the large eddy simulation, only the drag force was considered in this article. Other inter-phase interactions, such as the virtual mass force, may also be considered in future work. The two-fluid model coupled with the LES can be extended to the numerical simulation of other two-phase flows, such as liquid–solid, gas–solid and liquid–liquid flows.

Acknowledgments

The authors acknowledge the financial support from the National Natural Science Foundation of China (Nos. 20236050, 20676134, 50574081) and 973 Program (Nos. 2004CB217604, 2007CB613507).

Notation

b = Length of the blades, m
c_s = Smagorinsky coefficient
C_D = Inter-phase drag coefficient
d = Diameter of the bubble, m
D = Impeller diameter, m
Eo = Evotos number
F = body force, kg m^2 s^{-2}
g = gravity acceleration, m s^{-2}
G = turbulence generation rate, kg m^{-1} s^{-3}
G_e = extra source of turbulence due to bubble phase, kg m^{-1} s^{-3}
H_c = clearance of the impeller, m
k = kinetic energy, m^2 s^{-2}
N = impeller speed, rev·s^{-1}
p = pressure, Pa m^3 kg^{-1}
Re = Reynolds number
Ri = Richardson number ($Ri = \frac{k^2}{\varepsilon^2}\frac{u_\theta}{r}\frac{\partial(ru_\theta)}{\partial r}$)
S = strain-rate tensor, s^{-1}
t = time, s
T = tank diameter, m
u, $\mathbf{u}$ = velocity, m s^{-1}
u_{tip} = impeller tip speed, m
w = width of the blades, m
z = axial coordinate
α = gas holdup
ρ = density, kg m^{-3}
λ = Kolmogoroff microscale, m
μ = viscosity, kg m^{-1} s^{-1}
ω, $\boldsymbol{\omega}$ = angular velocity, rad s^{-1}
θ = angular coordinate, rad
τ = sub-grid stress, N m^{-2}
ν = kinematical viscosity, m^2 s^{-1}
δ = distribution function
ε = dissipation, m^2 s^{-3}
Δ = filter width, m

Subscripts

l, g = liquid and gas phase
b = bubble
eff = effective
i, j, k = principal direction
r, θ, z = cylindrical coordinate directions
b = bubble

Overbar

$\bar{}$ = space filtered

Literature Cited

1. Gosman AD, Lekakou C, Politis S, Issa RI, Looney MK. Multidimensional modeling of turbulent two-phase flows in stirred vessels. *AIChE J*. 1992;38:1946–1956.
2. Bakker A, van den Akker HEA. A computational model for the gas–liquid flow in stirred reactors. *Trans Inst Chem Eng*. 1994;72:594–606.
3. Ranade VV, Van Den Akker HEA. A computational snapshot of gas–liquid flow in baffled stirred reactors. *Chem Eng Sci*. 1994;49:5175–5192.
4. Morud KE, Hjertager BH. LDA Measurement and CFD modeling of gas–liquid flow in a stirred vessel. *Chem Eng Sci*. 1996;51:233–249.
5. Ranade VV, Deshpande VR. Gas–liquid flow in stirred reactors: trailing vortices and gas accumulation behind impeller blades. *Chem Eng Sci*. 1999;54:2305–2315.
6. Wang WJ, Mao Z-S. Numerical simulation of gas-liquid flow in a stirred tank with a rushton impeller. *Chinese J Chem Eng*. 2002;10:385–395.
7. Wang WJ, Mao Z-S, Yang C. Experimental and numerical investigation on gas holdup and flooding in an aerated stirred tank with rushton impeller. *Ind Eng Chem Res*. 2006;45:1141–1151.

8. Lane GL, Schwarz MP, Evans GM. Predicting gas–liquid flow in a mechanically stirred tank. *Appl Math Model*. 2002;26:223–235.
9. Lane GL, Schwarz MP, Evans GM. Numerical modeling of gas–liquid flow in stirred tanks. *Chem Eng Sci*. 2005;60:2203–2214.
10. Khopkar AR, Aubin J, Xureb C, Le Sauze N, Bertrand J, Ranade VV. Gas–liquid flow generated by a pitched blade turbine: PIV measurements and CFD simulations. *Ind Eng Chem Res*. 2003;42: 5318–5332.
11. Khopkar AR, Rammohan AR, Ranade VV, Dudukovic MP. Gas–liquid flow generated by a Rushton turbine in stirred vessel: CARPT/CT measurements and CFD simulations. *Chem Eng Sci*. 2005;60: 2215–2229.
12. Deen NG, Solberg T, Hjertager H. Flow generated by an aerated Rushton impeller: two phase PIV experiments and numerical. *Canadian J Chem Eng*. 2002;80:638–652.
13. Sun HY, Yu GZ, Mao Z-S. Experimental and numerical study of gas holdup in surface aerated stirred tanks. *Chem Eng Sci*. 2006;61: 4098–4110.
14. Eggels JGM. Direct and large-eddy simulation of turbulent fluid flow using the lattice-Boltzmann scheme. *Int J Heat Fluid Flow*. 1996;17:307–323.
15. Derksen J, van den Akker HEA. Large eddy simulations on the flow driven by a Rushton turbine. *AIChE J*. 1999;45:209–221.
16. Revstedt J, Fuchs L. Large eddy simulation of flow in stirred tanks. *Chem Eng Technol*. 2002;25:443–446.
17. Lu Z, Liao D, McLaughlin JB, Derksen JJ, Kontomaris K. Large eddy simulations of a stirred tank using the Lattice-Boltzmann method on a nonuniform grid. *J Comput Phys*. 2002;181:675–704.
18. Yeoh SLG, Papadakis KCL, Yianneskis M. Large eddy simulation of turbulent flow in a rushton impeller stirred reactor with sliding-deforming mesh methodology. *Chem Eng Technol*. 2004;27:257–263.
19. Alcamo R, Micale G, Grisafi F, Brucato A, Ciofalo M. Large-eddy simulation of turbulent flow in an unbaffled stirred tank driven by a Rushton turbine. *Chem Eng Sci*. 2005;60:2303–2316.
20. Zhang YH, Yang C, Mao Z-S. Large eddy simulation of liquid flow in a stirred tank with improved inner-outer iterative algorithm. *Chinese J Chem Eng*. 2006;14:321–329.
21. Wang QZ, Squires KD, Simonin O. Large eddy simulation of turbulent gas-solid flows in a vertical channel and evaluation of second-order models. *Int J Heat Fluid Flow*. 1998;19:505–511.
22. Apte SV, Gorokhovski M, Moin P. LES of atomizing spray with stochastic modeling of secondary breakup. *Int J Multiphase Flow*. 2003;29:1503–1522.
23. Afshari A, Shotorban B, Mashayek F, Shih TIP, Jaberi FA. Development and validation of a multi-block flow solver for large eddy simulation of turbulent flows in complex geometries. In: Proceedings of the 42nd AIAA Aerospace Sciences Meeting and Exhibit, 2004; 1492–1500.
24. Shotorban B, Mashayek F. Modeling subgrid-scale effects by approximate deconvolution. *Phys Fluids*. 2005;17:1–4.
25. Derksen J. Numerical simulation of solids suspension in a stirred tank. *AIChE J*. 2003;49:2700–2714.
26. Smith BL, Milelli M. An investigation of confined bubble plumes. *Presented at the Third International Conference on Multiphase Flow, ICMF'98*, Lyon, France, 1998.
27. Deen NG, Solberg T, Hjertager BH. Large eddy simulation of the gas-liquid flow in a square cross-sectioned bubble column. *Chem Eng Sci*. 2001;56:6341–6349.
28. Hjertager BH, Morud K. Computational fluid dynamics simulation of bioreactors. Proceedings of the Bioprocess Engineering Meeting. Stockholm, Lund, Sweden: Biotechnology Research Foundation, 1993;40–57.
29. Launder BE, Spalding DB. *Mathematical Models of Turbulence*. London: Academic Press, 1972.
30. Smagorinsky J. General circulation experiments with the primitive equations. I. The basic experiment. *Monthly Weather Rev*. 1963;91: 99–165.
31. Brucato A, Grisafi F, Montante G. Particle drag coefficients in turbulent fluids. *Chem Eng Sci*. 1998;53:3295–3314.
32. Lane GL, Schwarz MP, Evans GM. Modeling of the interaction between gas and liquid in stirred vessels. Proceedings of the 10th European Conference on Mixing, 2000;197–204.
33. Lu WM, Ju SH. Local gas holdup, mean liquid velocity and turbulence in an aerated stirred tank using hot-film anemometry. *Chem Eng J*. 1986;35:9–17.
34. Patankar SV. *Numerical Heat Transfer and Fluid Flow*. McGraw-Hill: New York, 1980.
35. Sagaut P. *Large Eddy Simulation for Incompressible Flows*. Springer-Verlag: Berlin, 2001.

Manuscript received July 5, 2007, and revision received Apr. 11, 2008.